RSC Advances

PAPER

View Article Online
View Journal | View Issue

Cite this: *RSC Adv.*, 2017, **7**, 19081

Nano-mechanical in-process monitoring of antimicrobial poration in model phospholipid bilayers†

Andrea Valsesia,*[a] Patrizia Iavicoli,[a] Helen Lewis,[b] Cloé Desmet,[a] Dora Mehn,[a] Luigi Calzolai,[a] Pascal Colpo,[a] François Rossi[a] and Maxim G. Ryadnov*[b]

Received 30th January 2017
Accepted 22nd March 2017

DOI: 10.1039/c7ra01274h

rsc.li/rsc-advances

Nanomechanical monitoring of known mechanisms of membrane poration mediated by host defense peptides is reported. Quartz Crystal Microbalance with Dissipation monitoring used to probe the process of antimicrobial poration in model phospholipid bilayers offers a straightforward method for mechanically differential kinetic measurements of membrane-mediated antimicrobial effects *in situ*.

Host defense or antimicrobial peptides (AMPs) are a major part of the innate immune system of all cellular organisms, from bacteria to humans.[1] The peptides are typically broad-spectrum antibiotics that recognize and target microbial membranes, including bacterial, fungal and viral. Unlike conventional antibiotics, AMPs do not differentiate between mature and growing bacteria, or between different types of bacteria, Gram positive or Gram negative, but destroy all.[2–4] Partly, this is because microbial cell walls as well as their membranes, phospholipid bilayers, are anionic, which allows these cationic peptides to bind to microbial cells. Partly, because AMPs fold into amphipathic conformations of α-helices or β-sheets, which allows them to intercalate in the hydrophobic interfaces of microbial phospholipid bilayers whereupon they assemble into membrane-disrupting pores and lesions causing cell lysis. Given that widespread resistance against them has yet to emerge, it is not surprising that AMPs are being considered as next-generation antimicrobial agents in the post-antibiotic era.[5] Similar to antibiotics, AMPs can engage with intracellular targets or disrupt processes that are crucial to the viability of microorganisms (protein, DNA, or cell wall syntheses). However, microbial membranes constitute the main and first line of attack for AMPs. This is the hallmark of their activity. Consequently, it is the interactions of these peptides with microbial phospholipid bilayers, their nature and extent that specify mechanisms of membrane disintegration. There appears to be several factors to consider that range from amino-acid compositions[6] to inoculum effects.[7] Yet, conformational responses to lipid binding remain the limiting and defining factors of antimicrobial mechanisms. Ultimately, these factors are encoded in structural features of peptide sequences and impact on antimicrobial activity. Questions remain as to the direct measurements of membrane-induced and folding-responsive antimicrobial mechanisms. These are necessary to expose mechanical processes that are fundamental to antimicrobial action, but are free of the constraints of live-cell measurements associated with other processes that are not necessarily involved in antimicrobial action.

Herein, we monitor and evaluate different poration mechanisms in the process of their development in real time. To achieve this while mitigating the complexities of live-cell measurements, the mechanisms were measured in reconstituted phospholipid bilayers, with lipid compositions supporting fluid-phase membranes at room and physiological temperatures. Anionic unilamellar vesicles (AUVs) mimicking microbial membranes were assembled from palmitoyloleoyl phosphatidylcholine (POPC) and palmitoyloleoyl phosphatidylglycerol (POPG) at 3 : 1 (molar) ratios. The vesicles were immobilised on the surfaces of quartz crystal for Quartz Crystal Microbalance with Dissipation monitoring (QCM-D) and were treated with peptides exhibiting distinctive mechanisms of action. Specifically, a synthetic peptide, tilamin, which was designed to lyse bacterial membranes by forming monolayer pits in their membranes[8] and a naturally occurring magainin 2, MAG-2, that forms transmembrane channels.[9–11] To compare these two established mechanisms (Fig. 1) each step difference was measured with QCM-D and correlated with morphological changes in vesicles determined by Atomic Force Microscopy (AFM) and Dark Field Microscopy (DFM).[12]

Results and discussion

Our approach is based on the recognition that QCM-D can probe mechanical differences in membranes by monitoring

[a]*European Commission – Directorate General Joint Research Centre Directorate F – Health, Consumers and Reference Materials – Consumer Products Safety, Via Fermi 2749 TP-125, 21027 Ispra, VA, Italy. E-mail: andrea.valsesia@ec.europa.eu*

[b]*National Physical Laboratory, Teddington TW11 0LW, UK. E-mail: max.ryadnov@npl.co.uk*

† Electronic supplementary information (ESI) available. See DOI: 10.1039/c7ra01274h

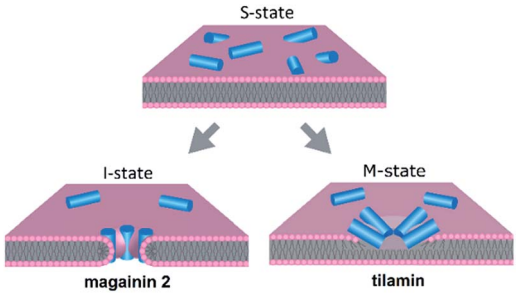

Fig. 1 Schematic of antimicrobial mechanisms in microbial phospholipid bilayers. Antimicrobial peptides (blue cylinders) bind to the surface of the membrane (S-state) and then either insert into lipid bilayers forming transmembrane pores (I-state) – magainin 2 – or porate the outer leaflet of the bilayer forming monolayer pores (M-state) – tilamin.

their adsorption and stability in real time. Rigidly bound layers can precisely follow the crystal's oscillatory motion, while weakly bound layers cannot, consequently inducing dissipative losses. It is thus possible to detect conformational changes in membranes by distinguishing individual adsorption stages. To enable this, real-time QCM-D curves were acquired continuously in two main steps.

Firstly, the kinetics and stability of liposomes immobilized on quartz crystals were monitored for 80 min after liposome immobilization and the removal of the unbound material. Secondly, this was directly followed by peptide injections at different concentrations with continuous monitoring for 240 min.

Surface deposition of intact liposomes

Liposomes used in the study had a *Z*-average value of 124 nm and a polydispersity index (PdI) of <0.15 indicating a monodisperse, uniformly sized distribution. QCM-D curves for the overtones indicated that liposomes formed a stable layer within the first 5 minutes of immobilization (Fig. 2). The variation of frequency, ΔF, proportional to the liposome adsorbed mass, was found to be in a range of −110 to −125 Hz, showing the good reproducibility of the used immobilization procedure. With a follow-up buffer injection, a slight decrease of mass was observed within the first 2 minutes, after which the QCM-D signal became constant. Gratifyingly, the results reflect the stability of the formed liposome layer and a negligible desorption rate. Such a rapid and stable adsorption of liposomes was indicative of strong interactions between the surface of anionic liposomes and the amine groups of a polydiallyldimethylammonium (PDDA) layer used to quench the surface functionalizing coating. The positive variation of the dissipation component ΔD over time supports the formation of a viscous layer on the functionalized quartz crystal. ΔD was at 15–20 × 10^{-6} d.u. at the end of the adsorption process

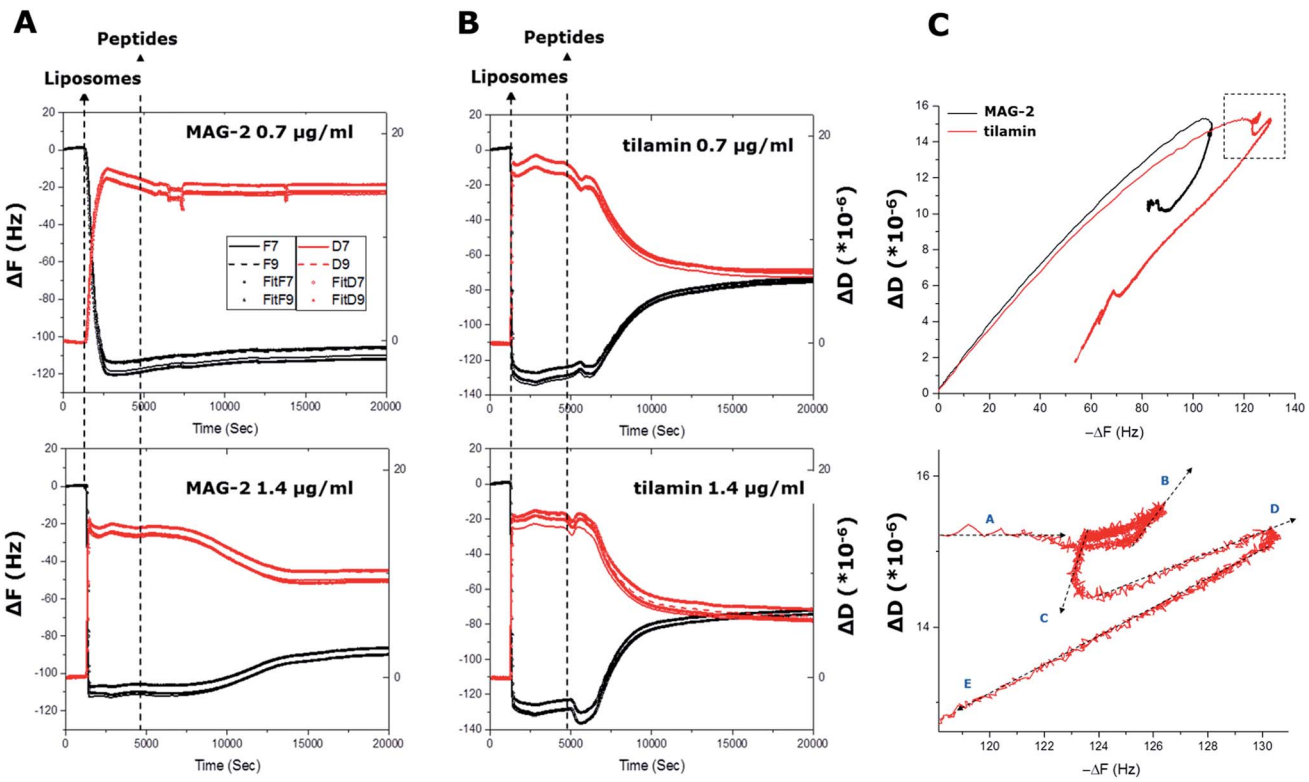

Fig. 2 In process monitoring of antimicrobial poration. (A) and (B) QCM-D curves (ΔF and ΔD) as a function of time from liposome adsorption (liposomes) to peptide injection at two different concentrations (peptides). Curves for all four cells of the quartz crystal used are shown. The ΔF and ΔD of two overtones (F7 and F9) are shown for each cell with corresponding fittings using the Voigt viscoelastic model (ESI†). (C) *F*–*D* plots of the four cells during the experiment for F9 overtone (upper) and a zoom of the circled area in (upper) for tilamin at 1.4 µg mL^{-1} (lower). The arrows indicate the temporal direction of the curves.

suggesting a monolayer formation of individual nano-spheres on the crystal surface.[13] Further evidence came from (i) constant increases in dissipation, up to the value of saturation, revealing that there was little or no liposome rupture, and (ii) steady decreases in the slopes of *F–D* plots (*D* variations monitored *versus F* variations), from 0.18 s to 0.15 s, confirming that the adsorbed layer was nearly complete and stabilized. In addition, the linear part of the plot curves showed that each liposome contributed to the variation of the dissipation factor by increasing the viscosity of the layer. Since no apparent changes were observed in the first phase of the adsorption both immobilized liposomes and their monolayer were deemed intact.

To gain an insight into the mechanical properties of the monolayer formed, we applied the Voigt model to interpret the results. The model allows determining the viscosity (V_{layer}) and thickness (Th_{layer}) of the layer by fitting the QCM-D frequency and dissipation curves as a function of the layer density (D_{layer}) and the shear elastic (E_{layer}) modulus of the liposomes. The viscoelastic modeling of D_{layer} was carried out by fixing the mass density of the liposomes and E_{layer}, the values of which were obtained by sedimentation velocity measurements (see ESI†). Fitting was performed using *F–D* curves from two overtones (F7 and F9), with D_{layer} and E_{layer} used at fixed values, and V_{layer} and Th_{layer} being variable. The fitting returned consistent decreases in liposome thickness of 53–58 nm against 124 nm measured by dynamic light scattering (DLS). The results suggest that liposomes flatten or halved in size upon immobilization or do not form a complete, homogeneous monolayer. AFM measurements confirmed that liposome deposition resulted in liposomes being evenly distributed on the surface, with diameters and heights being 150 ± 42 nm and 122 ± 7 nm, respectively (Fig. S1†). Thus, the parameters appeared consistent with the diameters measured by DLS, indicating that the liposomes remain intact in a discrete monolayer. Collectively, the results confirm that liposomal adsorption on the substrates did not result in modifications of the lipid bilayer, even within several hours post-adsorption, thus amply supporting QCM-D as a direct method for probing the mechanics of known membrane poration mechanisms.

Monitoring antimicrobial poration in process

To confirm antimicrobial activities, both peptides were tested against bacteria using microdilution assays, with returned Minimum Inhibitory Concentration (MIC) typical of polypeptide antibiotics (see ESI†). A cross-comparison in the activities of the two peptides revealed no apparent preference for Gram positive (*S. aureus*, *B. subtilis*) or Gram negative (*E. coli*, *S. enterica*) bacteria. Tilamin proved to be equally active against all the bacteria with low-range MICs (1–10 μM). Similarly, MICs for magainin 2 were comparable, albeit higher (>50–100 M), across the same bacteria with an exception of *B. subtilis* (<5 μM). Consistent with earlier reports,[8,14] these differences did not appear systematic to discriminate one type of bacteria against the other and are likely due to phenotypic tolerance of bacteria to antibiotics.[15]

To monitor membrane changes the monolayer was exposed to the two peptides. At the both concentrations used decreases in frequency ($\Delta F < 0$) and dissipation ($\Delta D < 0$) were evident for tilamin, with more apparent effects observed for higher concentrations. A sharp negative *F* decay of 7 Hz started at 5000 s and developed over 600 s. Complementary to this were decreases in *D* that developed from 15.2×10^{-6} to 14.4×10^{-6} units within 500 s at 4600 s.

Further, in *F–D* plots in the region of −118 to −122 Hz, ΔD remained constant at 15.2×10^{-6}, corresponding to the maximum mass of liposomes adsorbed. However, five different mechanical phases (A–E) could be identified in the region (Fig. 2C). Specifically, with ΔF decreasing, ΔD remains constant at 15.2×10^{-6} in phase A. This is a terminal phase in the formation of a stable monolayer. In phase B, *F* remains constant while ΔD increases to 15.6×10^{-6}. This phase corresponds to the attachment of the first tilamin monomers on membranes, and, when compared to undetectable mass changes, the observed increases indicate a very strong mechanical change induced by pore-forming peptides. Phase C follows with decreases in both ΔD (14.6×10^{-6}) and ΔF, which correspond to the re-organization of the lipid bilayers upon peptide insertion, leading to stabilized liposomes. Increases in ΔD (15.0×10^{-6}) and ΔF in phase D, reflect the progressive accumulation of the peptides in forming and merging pores. The latter is more apparent in phase E, where ΔD and ΔF are both decreasing, indicating the progressive disruption of liposomes. In marked contrast, only two phases of the ΔD were evident for MAG-2, indicating a one-phase transition from peptide insertion to liposomal disruption. The results are striking in that MAG-2 is indeed prone to promote homogeneous transmembrane pores,[14] while tilamin thins the outer leaflets of phospholipid bilayers *via* the formation of coalescent monolayer pores.[8]

To provide further evidence into the observed differences the adsorption of tilamin and MAG-2 was fitted using the same viscoelastic model. Upon membrane binding tilamin induced a very small decrease in liposome thickness (a negative variation of 5 nm is fitted in the model), but a strong and immediate increase in the viscosity of the outer leaflet of the bilayer (2% increase of its original value) (Fig. 3).

Such an increase supports a major structural change in the liposome monolayer, with similar effects in liposome viscosity commonly found for membrane-inserting proteins and peptides that cause membrane disruptions by introducing liquid ordered phases.[16] Thus, tilamin insertion and rapid assembly in the bilayer increased its hydrophobic mismatch and consequently viscosity, lowering membrane viscosity and resulting in bilayer rupture. A membrane disruption phase was also apparent for MAG-2 at high concentrations, with no appreciable effects detected at lower concentrations. The thickness decreased by 20 nm (from 123 nm to 103 nm), whereas the relative change of thickness was much lower than that for tilamin. To better illustrate the different mechanisms of the two peptides, a column scatter plot was built displaying the fitted values for corresponding thickness and viscosity at the two different concentrations (Fig. 3E and F). Variations in both viscosity and thickness were visibly broader for tilamin-membrane interactions.

The mechanical properties of peptide-treated membranes proved to correlate with the morphological changes of liposomes. AFM measurements revealed weak (soft) force responses

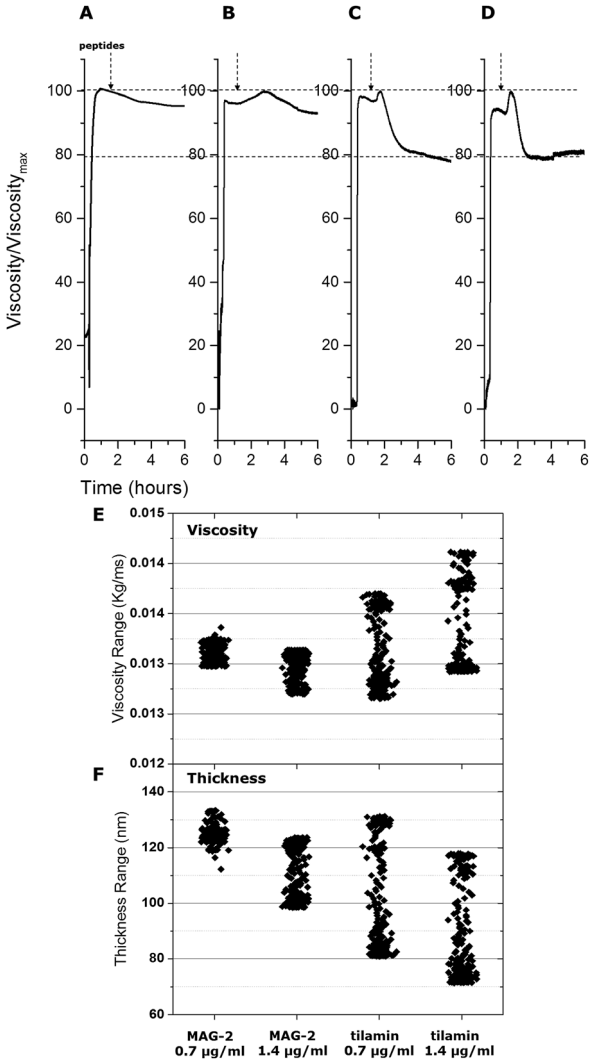

Fig. 3 Monitoring antimicrobial poration as a function of membrane thickness and viscosity. (A–D) Viscosity (bottom) measured at the quartz surface for the four cells during step number 2, after the injection of the peptides. The values as a function of time are the result of the fitting of F7 and F9 overtones using the Voigt model. The variation of viscosity had been normalized to the initial value for each sensor. (E, F) Column scatter plots for the fitted viscosity and the thickness for the four cells for the whole experiment.

of liposomes even when soft cantilever were used under the softest conditions (Materials and Methods in ESI†). The liposomes were round-shaped, 122 ± 7 nm in height and 150 ± 42 nm in diameter, thus agreeing with the results from the DLS measurements. Larger diameters found by AFM are attributed to that AFM measurements are intrinsically prone to overestimate lateral parameters. Peptide treatments (40 min) reduced the liposomes to a diameter of 31 ± 11 nm, which was consistent with the mass loss obtained by QCM-D. Amorphous structures, irregular in shape, became apparent as a likely result of peptide-caused membrane disruption. Following prolonged treatments (2 hours) led to liposomes coalesced into larger aggregates (Fig. S1†). As further gauged by a dark field microscopy in real time, the aggregates appeared to be collapsed, ring-shaped liposomes (Fig. S2†).

Conclusions

We have described the design and application of QCM-D monitoring to probe membrane-mediated antimicrobial activity. The method enabled the nanoscale mechanical evaluation of antimicrobial mechanisms in process, *in situ* and in real time in model phospholipid bilayers. To the best of our knowledge, this is the first example of differential mechanical and kinetic measurements of antimicrobial effects in phospholipid bilayers. Our approach allows for differentiating between distinctive, but closely related, poration mechanisms. The detection of several mechanical phases for tilamin confirmed a unique mode of action that is different from that of MAG-2, which was characterized by a two-phase transition. In both cases bilayer rupture was shown to result from localized poration thus supporting the generic mechanism of host defence peptides as physical membrane-active antibiotics.[4,17] In this regard, the developed method offers an empirical tool for the *in situ* monitoring of antimicrobial effects and for the direct assessment of anti-microbial activity that may underpin new capabilities for screening membrane-active antimicrobial agents.

Acknowledgements

We acknowledge funding from the European Metrology Research Programme (EMRP) projects. The EMRP is jointly funded by the EMRP participating countries within EURAMET and the European Union.

Notes and references

1 K. A. Brogden, *Nat. Rev. Microbiol.*, 2005, **3**, 238–250.
2 Y. Sang and F. Blecha, *Anim. Health Res. Rev.*, 2008, **9**, 227–235.
3 H. Sato and J. B. Feix, *Biochim. Biophys. Acta, Biomembr.*, 2006, **1758**, 1245–1256.
4 C. D. Fjell, R. E. W. Hancock and A. Cherkasov, *Bioinformatics*, 2007, **23**, 1148–1155.
5 J. L. Fox, *Nat. Biotechnol.*, 2013, **31**, 379–382.
6 P. D. Rakowska, *et al.*, *Proc. Natl. Acad. Sci. U. S. A.*, 2013, **110**, 8918–8923.
7 A. K. Jepson, J. Schwarz-Linek, L. Ryan, M. G. Ryadnov and W. C. K. Poon, *Adv. Exp. Med. Biol.*, 2016, **915**, 33–48.
8 A. Pyne, *et al.*, *Chem. Sci.*, 2017, **8**, 1105–1115.
9 Y. Imura, N. Choda and K. Matsuzaki, *Biophys. J.*, 2008, **95**, 5757–5765.
10 Y. Huang, J. Huang and Y. Chen, *Protein Cell*, 2010, **1**, 143–152.
11 M. Zasloff, *Proc. Natl. Acad. Sci. U. S. A.*, 1987, **84**, 5449–5453.
12 J. M. Nascimento, O. L. Franco, M. D. Oliveira and C. A. Andrade, *Chem. Phys. Lipids*, 2012, **165**, 537–544.
13 D. Johannsmann, I. Reviakine and R. P. Richter, *Anal. Chem.*, 2009, **81**, 8167–8176.
14 S. J. Ludtke, K. He, W. T. Heller, T. A. Harroun, L. Yang and H. W. Huang, *Biochemistry*, 1996, **35**, 13723–13728.
15 F. Corona and J. L. Martinez, *Antibiotics*, 2013, **2**, 237–255.
16 G. Guigas and M. Weiss, *Biophys. J.*, 2008, **95**, L25–L27.
17 Y. Shai, *Pept. Sci.*, 2002, **66**, 236–248.